Innovative Infrastructure Solutions (2020) 5:108
https://doi.org/10.1007/s41062-020-00356-1

TECHNICAL PAPER

Influence of bauxite residue (red mud) on corrosion of rebar in concrete

U. Raghu Babu[1] · **B. Kondraivendhan**[1]

Received: 13 June 2020 / Accepted: 17 August 2020 / Published online: 1 September 2020
© Springer Nature Switzerland AG 2020

Abstract

This paper examines the corrosion of rebar embedded in concrete when cement is partially replaced with toxic bauxite residues, known as red mud (RM). The concrete mixtures were made with 100% ordinary Portland cement (OPC), and OPC replaced with 5% of RM (95% OPC + 5% RM). In order to evaluate the rebar corrosion in aforesaid concrete mixes, 5% calcium chloride was admixed while preparing the concrete. The corrosion performance of rebar in OPC concrete and concrete blended with RM was monitored by corrosion potential and linear polarization resistance. In addition, the performance of concrete blended with RM is evaluated through IR (Ohmic drop) compensated electrical resistivity. After 420 days of corrosion monitoring, concrete samples were broken, and visual observations were made on the rebar. X-ray powder diffraction analysis is also carried out on concrete powder samples collected from the steel–concrete interface. The experimental results have shown that the RM blended concrete performed better to resist the corrosion of rebar as compared to OPC concrete across the testing period of 420 days in the case of concrete made of w/cm 0.48. However, the overall corrosion current density increased in RM blended concrete as compared to normal concrete for the w/cm 0.51.

Keywords Concrete · Calcium chloride · Corrosion · Rebar · Red mud · Electrical resistivity · LPR

Introduction

Alumina from bauxite ore is the raw material for aluminum production [1]. According to the International Aluminum Institute (IAI), production of aluminum across the world has reached 60.4 million tonnes in 2020, which will increase in the coming years [2]. Each ton of alumina production generates approximately 1 to 1.5 tonnes of bauxite residue, generally known as red mud (RM). Continuous and robust growth of alumina production alarms environmental, safety issues, and the disposal problems of hazardous RM as well. RM is disposed of by various methods like pumping, sea dumping, and landfill into storage dams [3]. Failure or leakage of storage dams due to heavy rains can lead to social and environmental contamination when hazardous and toxic bauxite residue is dumped into the ponds or storage dams. The accident due to the failure of red mud reservoir of the Timfoldgyar alumina plant (Ajka, Hungary) witnessed the importance to safeguard red mud storage dams. Because RM is considered a highly toxic residue, leakage becomes a severe problem for communities living around the alumina refinery. Storage and environmental issues related to RM and its large-scale production attract researchers to explore the sustainable possibilities of utilization of bauxite residues.

Singh et al. [4] investigated the influence of RM on durability and mechanical properties of geopolymer paste made with fly ash and different dosages of RM. They reported that the geopolymer paste containing the red mud up to 30% performed better against sulfuric and acetic acid solution. However, the higher alkalinity, lesser calcium, and aluminum content are also helpful for its higher resistance against sulfuric and acetic acid attack. Based on the studies conducted by Díaz et al. [5], it was mentioned that low chloride ions diffusion in RM blended cement paste is due to high aluminum content, which traps the chlorides. Díaz et al. [5] also reported that the high amount of calcium silicate hydrate (CSH) gel developed in RM mixtures retained the carbon dioxide (CO_2) penetration. Based on the electrochemical and surface characterization techniques, Díaz et al.

✉ U. Raghu Babu
ammaraghubabu@gmail.com

B. Kondraivendhan
bkv@amd.svnit.ac.in

[1] Civil Engineering Department, Sardar Vallabhbhai National Institute of Technology, Surat, Gujarat 395007, India

[5] emphasize the passivation behavior of RM particles in alkaline media, which increases the corrosion resistance of carbon steel subjected to a large amount of chloride. Singh et al. [4] attributed the beneficial effects of RM with the higher alkalinity and lower aluminum content. On the other hand, Díaz et al. [5] attributed the higher chloride trapping due to high aluminum content. The reason for differences of RM behavior is owing to the composition of RM which changes from place to place due to the various factors like the type of bauxite ore, aluminum production process, etc.

Cabeza et al. [6] investigated the reinforcement corrosion inhibition effect of RM in model solutions and in mortar specimens contaminated with calcium chloride ($CaCl_2$). It is reported by Cabeza et al. [6] that the RM helps to form a thinner protective film on the rebar. It means that the presence of RM in chloride contaminated mortar mix able to resist the depassivation of rebar. Based on the results of cyclic voltammetry and electrochemical impedance spectroscopy studies, Collazo et al. [7] reported the effectiveness of RM to resist corrosion of reinforcement. They also reported that rebar in RM solution maintains the passivity up to 90 days, while in solutions of sodium hydroxide (NaOH) and calcium hydroxide ($Ca(OH)_2$) with the same pH, at 25 and 55 days pit formation was observed. Yang et al. [8] mentioned that the addition of RM up to 6% with cement could enhance the compressive strength. This effect was due to the densification of microstructure, which was confirmed by the decrease in $Ca(OH)_2$ content when there was an addition of RM. With the help of a heavy metal leaching test, Yang et al. [8] stated that the utilization of RM for the mortar matrix is not harmful and one can use it in cement works without any fear. The recent publications of Venkatesh et al. [9, 10] reported that the replacement of cement with RM up to 10% enhances the concrete strength and durability.

Nikbin et al. [11] reported that the addition of RM by 25% decreased the ultrasonic pulse velocity values, compressive, flexural and split tensile strength values and increased the absorption capacity of water, but that the concrete properties too remained in the acceptable range. Nikbin et al. [11] stated that the environmental impacts were decreased with the incorporation of RM. Manfroi et al. [12] described the pozzolanic reactivity of RM, and the replacement up to 5% of RM which is calcined at 600 °C was suggested as the most appropriate replacement % of cement. Ribeiro et al. [13] evaluated the replacement (10, 20, and 30%) of RM and its effect on corrosion resistance of rebar in concrete based on half-cell potential, chloride diffusion, and concrete resistivity. The results showed that the replacement of RM increased the electrical resistivity and corrosion resistance of rebar.

$CaCl_2$ is the most widely used to accelerate the setting and hardening of concrete, due to its low cost and ready availability. However, the utilization of $CaCl_2$ has been questioned since it accelerates the possibility of rebar corrosion. To investigate the effect of chloride-induced corrosion, researchers widely used sodium chloride (NaCl) and $CaCl_2$ in their studies. At the same amount of chlorides, $CaCl_2$ is more aggressive than NaCl. NaCl promotes corrosion only, but $CaCl_2$ can also attack the cement matrix [14]. The $CaCl_2$ restrained the ionization of calcium hydroxide, thus resulting in a low pH concrete pore solution. At the same time, $CaCl_2$ binds more chlorides, which favors decreasing the corrosion effect, since only free chlorides are responsible for corrosion [15]. Earlier studies reported that the composition of cementitious material strongly influences the presence of free chlorides [16–18]. High amounts of free alkali, gypsum, and less amount of alumina and ferric oxide increase the content of free chlorides in concrete [19]. The purpose of the current investigation is to determine the effect of RM on the corrosion performance of embedded rebar when $CaCl_2$ is admixed with concrete during concrete production.

Experimental study

Materials and specimen preparation

To examine the influence of red mud on the corrosion performance of rebar embedded in concrete, concrete prepared with ordinary Portland cement (OPC) 53 grades which conform to Indian Standard IS12269:2015 is compared with concrete made with binder composed of 95% of OPC and 5% of RM. The chemical composition of OPC and RM is shown in Table 1. Due to limited available literature on the incorporation level of RM in concrete and its effect on corrosion, the investigation has been conducted [12]. To examine the influence of water to cementitious material (w/cm) ratio on corrosion behavior of concrete, two w/cm ratios, such as 0.48 and 0.51, were used. Higher w/cm ratios were considered to expedite the corrosion process and to complete

Table 1 Chemical composition of cementitious materials

Chemical compound (%)	Al_2O_3	Fe_2O_3	SiO_2	TiO_2	CaO	MgO	Na_2O	SO_3	[a]LOI
OPC	5.32	4.23	20.65	–	64.12	1.13	–	2.16	2.39
RM	16.15	54.8	6.3	3.7	1.98	1.0	3.55	0.72	11.8

[a]*LOI* Loss of ignition

Table 2 Concrete mix proportion

w/cm	Constituents (kg/m^3)	Ordinary Portland cement	Red mud
0.48	Cement	395.83	376.04
	Pozzolan	–	19.79
	Coarse aggregate	1034.72	1034.44
	Fine aggregate	849.95	849.71
0.51	Cement	372.55	353.92
	Pozzolan	–	18.62
	Coarse aggregate	1045.96	1045.63
	Fine aggregate	859.13	858.91

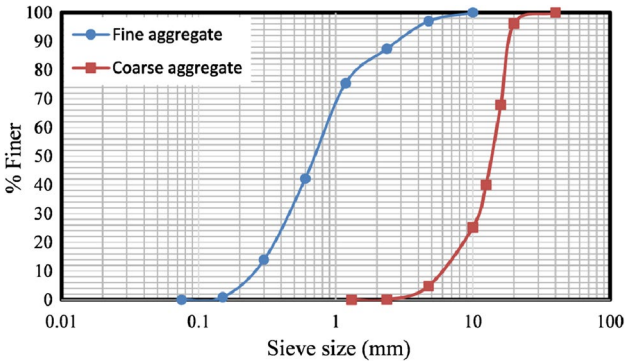

Fig. 1 The gradation curve for fine and coarse aggregates

the investigation within the stipulated time period. Four concrete mixes were made with two w/cm ratios and two cementitious materials. The concrete mix proportions are given in Table 2. The coarse aggregate of 20 mm maximum size aggregate (MSA) and 10 mm MSA was used in the ratio of 60% and 40% of the total mass of coarse aggregate, respectively. Locally available sand confirming to grading Zone II was used as fine aggregate. The gradation curve for fine and coarse aggregate is shown in Fig. 1. Laboratory tap water with 5% of calcium chloride was used as mix water for concrete preparation. Thermomechanically treated rebar of diameter 10 mm, and length 360 mm was used as reinforcing steel. One end of the rebar is threaded to attach one screw and two nuts of stainless steel for electrical connections. The rebars were cleaned with sulfuric acid and water, followed by wire brushing as per the ASTM G109-99a [20]. The rebar after cleaning is shown in Fig. 2a. Both ends of the rebar were taped with electroplaters tape, leaving the middle portion of length 250 mm for exposure. Neoprene tubes were placed over the tape, and the ends were sealed with epoxy, as shown in Fig. 2b.

Reinforced slab specimens of size 320 mm × 320 mm × 21 mm embedded with 10 mm rebar were cast for corrosion monitoring. The pictures of slab molds and the preparation of slab specimens are shown in Fig. 2c and d, respectively. After 24 h, the reinforced slab samples were removed from molds and exposed to moist

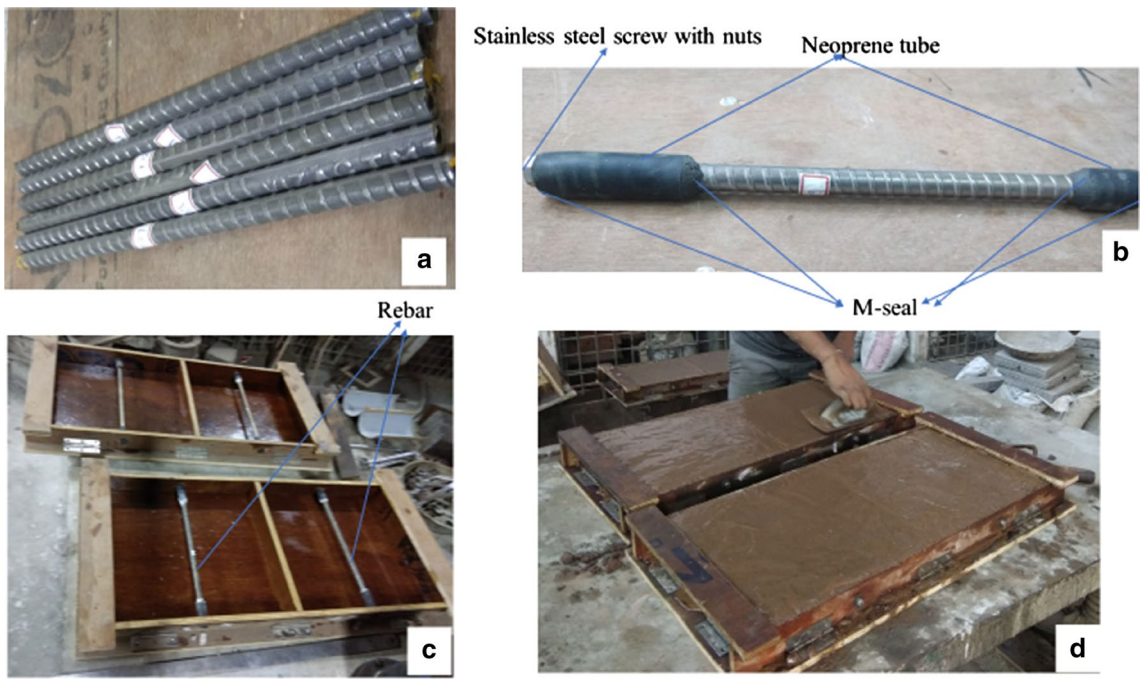

Fig. 2 The picture of **a** Rebars after cleaning as per ASTM G109-99a [20], **b** Rebar prepared to place in concrete, **c** Slab specimen molds with rebars at center **d** Casting of reinforced slab specimens

curing for 27 days. The specimens at the age of 28 days were removed from the curing tank and exposed to ambient laboratory conditions till the day of testing.

Test techniques

After moist curing, the 28 days old specimens were removed and allowed to dry for 2 days in laboratory conditions before conducting the electrochemical studies for the first time. It helps to minimize the error caused by too much wetness. The corrosion parameters were monitored on reinforced slab specimens for a period of 420 days at the cycle of 30 days. From second cycle onwards, to minimize the errors due to excessive dryness, the slab specimens were subjected to wetting for 10 h prior to commencing the test. Nondestructive electrochemical studies were conducted on the reinforced slabs with a corrosion monitoring instrument (ACM Gill AC guard serial no. 1824), which is provided with the guard ring, as shown in Fig. 3. The influence of RM on corrosion of rebar is evaluated by corrosion potentials and corrosion current density values (I_{corr}). I_{corr} values were measured by linear polarization resistance (LPR) technique. Besides, the electrical resistivity of reinforced slab specimens was measured by Ohmic drop compensation. Since the concrete electrical resistivity is not the definitive measure of corrosion, in this study, it is used as a complement to other corrosion studies.

Corrosion potentials

The measurement of half-cell potential or corrosion potential is a well-known and most widely used electrochemical method to assess the rebar corrosion risk. It measures the potential difference between the rebar and a reference electrode. In this study, corrosion potential of the rebar embedded in concrete is measured over 420 days using saturated calomel electrode (SCE) as a reference electrode. In order to provide the proper ionic conduction, the sponge soaked with soap water is placed in between the surface of concrete and SCE. The potentials were measured by placing the SCE just above the concrete surface and parallel to rebar at five different points. The corrosion potential is considered as the average of five readings. The probability of corrosion is evaluated from the corrosion potential-time plot, as per the ASTM C876 [21], a criterion of − 275 mV SCE.

Corrosion current density

LPR technique can give the quantitative information about the rebar corrosion in terms of polarization resistance. A small potential scan in the range of − 20 to + 20 mV of the corrosion potential with a scan rate of 0.1 mV/s was used to determine the polarization resistance (R_p). To increase the accuracy of results, the current is confined to a specific surface area of rebar by using a guard ring setup. The particulars of the guard ring setup are detailed elsewhere [22, 23]. The high resistance of concrete causes the error in corrosion results due to ohmic drop (IR) between SCE and rebar. To avoid this error, R_p values were measured for the IR-compensated LPR technique. I_{corr} values were determined from the measured polarization resistance by Stern and Geary formula:

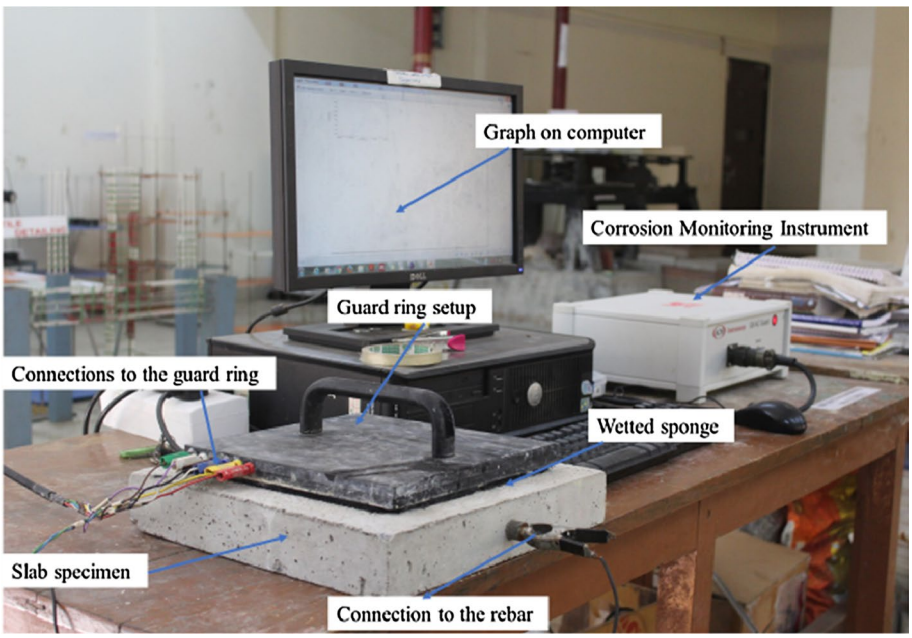

Fig. 3 Corrosion monitoring instrument with guard ring setup

$$I_{corr} = B/R_p \quad (1)$$

Here, I_{corr} is the corrosion current density, μA/cm^2; R_p is the polarization resistance of reinforcing steel, KΩ cm^2; and B is the Stern–Geary constant

$$B = \frac{(\beta_a X \beta_c)}{2.3(\beta_a + \beta_c)} \quad (2)$$

β_a and β_c are the anodic and cathodic Tafel constants, mV/decade, respectively.

In the absence of tafel constants data for rebar embedded in concrete, it is commonly taken B value as 26 mV for active and 52 mV for passive conditions [24, 25]. In this study, B value is adopted as 26 mV for the measurement of I_{corr} values.

IR-compensated electrical resistivity

The instrument used in the current investigation can measure the IR drop between the rebar and the reference electrode. Generally, ohmic drop or IR drop is referred to the resistance offered by the concrete media during the flow of electrical current. Ahmad and Bhattacharjee [26] reported that the ohmic resistance of concrete could be used as an approximate estimate of the concrete electrical resistivity. Samson et al. [27] proposed a model based on the link between the ohmic drop and concrete resistivity. Pradhan and Bhattacharjee [28] also discussed the resistivity of concrete based on the measured IR-compensated value. Since the distance between the electrodes maintained the same throughout the testing period, the resistance of cover concrete was measured using IR-compensated resistance.

Results

Corrosion potentials

As shown in Fig. 4, in concrete made of w/cm 0.48, the rebar in OPC and RM blended concrete reaches the more active potentials than the threshold potential of −275 mV SCE as specified by ASTM C876 [21] before 60 days. The same can be observed in the concrete made with w/cm 0.51. That is to say that the presence of chlorides at the concrete preparation did not allow to passivate the rebar, or there is no stable passive layer was formed in the calcium chloride contaminated concrete.

The potential values were more negative and reached more than −650 mV in w/cm 0.48 and −550 mV in case of w/cm 0.51 and then moved toward positive values. The similar trend of potentials, i.e., moving toward to positive direction can also be observed by Vedalakhmi et al. [29]

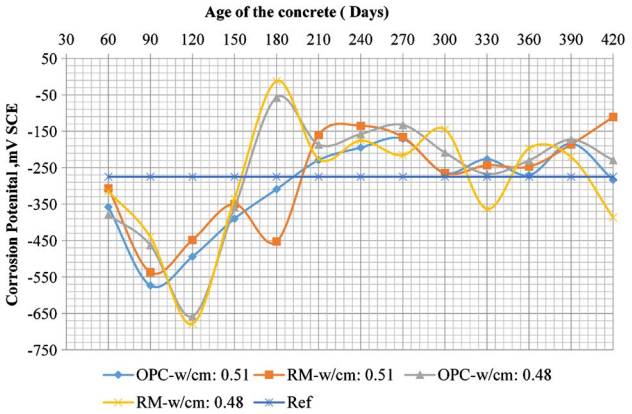

Fig. 4 Corrosion potentials on rebar embedded in OPC concrete and concrete made with RM for both w/cm ratios 0.48 and 0.51

in the cases of reinforced concrete specimens made with Portland pozzolan and Portland slag cement. In w/cm 0.48, rebar shows negative potential than threshold potential up to 150 days and then the potential values shifted to positive direction. Nevertheless, in the case of concrete with w/cm 0.51, the rebar shows negative potential up to 180 days. This can be attributed to changes of microstructure over the time and the availability of free chlorides. It is also observed that the rebar in concrete with w/cm 0.51 shows active potential (negative than threshold) values for longer period as compared to rebar in concrete with w/cm 0.48. With these outcomes, it can be noted that even a small change in w/cm ratio can influence the potential values. While observing the effect of cementitious material on potential values, no significant difference was observed in both w/cm 0.48 and 0.51. Figure 4 indicated the behavior of potential trend with time keeps on varying. This may be due to the influence of several factors such as temperature, humidity, oxygen availability, and resistance of concrete on corrosion potential at the time of measurement.

Corrosion current density values

The variation of I_{corr} data with time for rebar embedded in concrete made with OPC and RM is shown in Fig. 5. The I_{corr} values shown in Fig. 5 were derived from polarization resistance values measured from IR-compensated LPR technique. While observing the influence of w/cm on I_{corr} values, the higher corrosion current values were found in the reinforced slabs made with w/cm 0.51, as compared to those made with w/cm 0.48. It is also observed that the I_{corr} values are not increasing with the time significantly in concrete with w/cm 0.48, whereas slight variation can be observed in w/cm 0.51 across a period of 420 days.

Over a period of 420 days, the maximum and minimum I_{corr} values reached by rebar in OPC concrete with w/cm

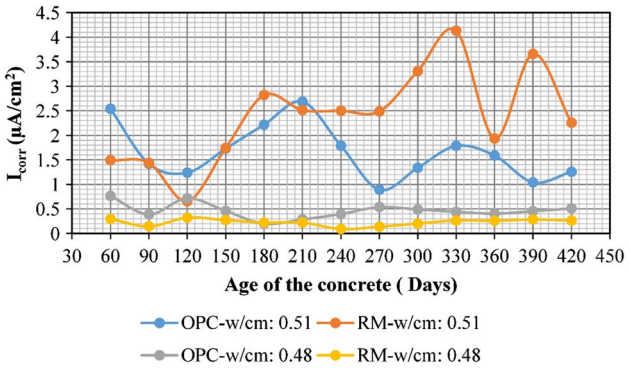

Fig. 5 Variation of I_{corr} of rebar embedded in concrete made with OPC and RM for w/cm 0.48 and 0.51

0.51 were 2.7 μA/cm^2 and 0.9 μA/cm^2, respectively, whereas the same for RM concrete are 4.1 μA/cm^2 and 0.6 μA/cm^2, respectively. It means that the concrete made with w/cm 0.51 presents the large variability in I_{corr} data with time as compared to concrete made with w/cm 0.48. Figures 5 and 6 depict the influence of RM on I_{corr} data of rebar in different w/cm ratios namely 0.48 and 0.51. It is also observed from Fig. 5, in the case of w/cm ratio 0.51, rebar in RM blended concrete shows almost less corrosion initially as compared to OPC concrete, but I_{corr} value of rebar in RM blended concrete increased significantly over the time. Over a period of 420 days of corrosion monitoring on specimens made with w/cm 0.48, the difference between I_{corr} values of OPC and RM blended concrete is not significant. The overall performance of concrete with two cementitious materials and two w/cm ratios on the corrosion of rebar can be understood more clearly through Fig. 6. The mean values of I_{corr} data measured on rebar embedded in OPC concrete

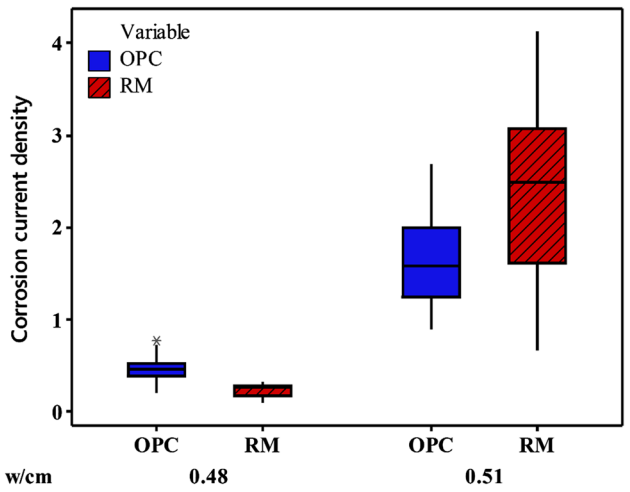

Fig. 6 Box plot of corrosion current density values of rebar in concrete made with OPC and RM

and RM blended concrete for w/cm 0.48 are 0.47 μA/cm^2, and 0.23 μA/cm^2, respectively. For w/cm 0.51, the mean I_{corr} values are 1.65 μA/cm^2 and 2.4 μA/cm^2 for OPC and RM blended concrete, respectively.

IR-compensated electrical resistance

The IR-compensated electrical resistivity versus time for the specimens made with OPC and RM blended concrete is shown in Fig. 7. The resistivity values shown on the plot correspond to the average of three replicates. Generally, the resistivity of concrete is used as an indicator of the corrosion of rebar [30, 31]. An oversimplified interpretation of concrete resistivity value is described as below [32]:

Electrical resistivity (kΩ cm)	Probability of corrosion
< 5	Very high
5–10	High
10–20	Low to moderate
> 20	Low

It can be seen from Fig. 7, that the electrical resistivity of all concrete mixes was almost lower than the 5 kΩ cm except concrete made with OPC and w/cm 0.48. It implies that the rebar embedded in all concrete mixes is prone to very high corrosion. An increase in electrical resistivity with time can be observed in all concrete mixes, mostly up to the age of 270 days, thereafter decreasing trend can be seen. While observing the effect of w/cm ratio on concrete electrical resistivity, the rise in w/cm ratio decreases the resistivity of concrete in both concrete made with OPC and RM as expected. Due to the change in available moisture content in concrete, the fluctuations can be observed in the electrical resistivity of the concrete over the time. The influence of RM on the concrete electrical resistivity is observed in

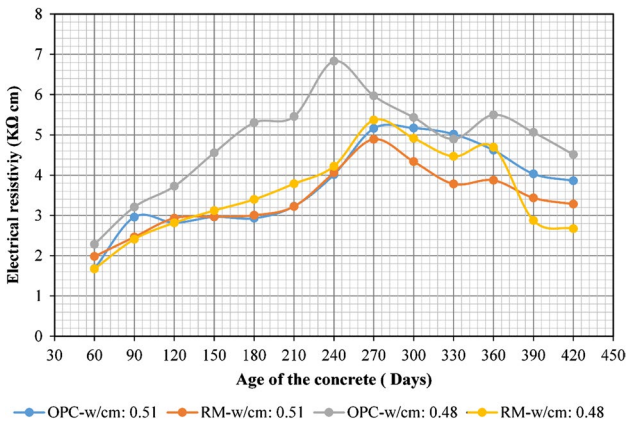

Fig. 7 IR-compensated electrical resistivity of concrete made with OPC and RM for w/cm 0.48 and 0.51

Fig. 7. According to Fig. 7, concrete made with RM shows lower electrical resistivity as compared to OPC concrete for both the w/cm ratios 0.48 and 0.51.

X-ray powder diffraction (XRPD) analysis

As shown in Fig. 8, the hydration products of concrete admixed with $CaCl_2$ are calcium chloro-aluminate (Friedel's salt), quartz, calcium hydroxide, calcium carbonate, and calcium hypochlorite. In addition, some amounts of ettringite can be observed in XRPD maps at 25.6° 2θ and 27.5° 2θ (Powder diffraction file 00-041-1451, ICDD). This formation of ettringite is due to the reaction of hydrated calcium aluminate and gypsum, which was added during the cement production to control initial setting time. Thaumasite observed at 27.5° 2θ on the XRPD map can be formed either by the direct route, i.e., from the reaction among CSH, Ca^{2+}, $CO_3^{-2,}$ and SO_4^{-2}, or indirect from ettringite like woodfordite and heterogeneous nucleation on the surface of ettringite. The direct formation of thaumasite is still not clear. When comparing the thaumasite peak intensities of concrete made with OPC and RM for w/cm ratio 0.51, it can be observed that the thaumasite peak intensity is higher in OPC as compared to RM blended concrete. However, the opposite trend can be seen when ettringite peak intensities of concrete made with OPC and RM are compared. During the hydration process, ettringite can be formed based on the availability of sulfate ions and aluminates. The formation of ettringite ceases once the aluminate is fully consumed, and then, thaumasite precipitation starts. Hence, the presence of high amount of aluminates and ferrites in RM as compared to OPC favors the higher ettringite fraction.

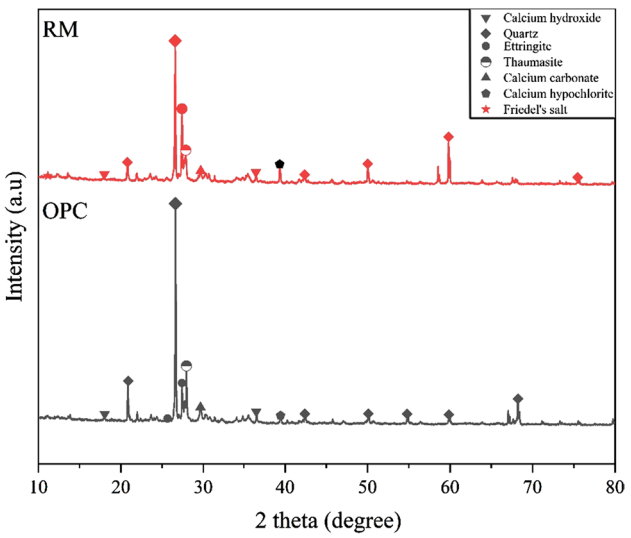

Fig. 8 XRPD map of $CaCl_2$ admixed concrete samples of OPC and RM for w/cm ratio 0.51

Since thaumasite formed due to reaction of gypsum with calcium carbonates and CSH gel, high sulfate content in OPC as compared to RM also favors for higher thaumasite fraction in OPC. Aggregates in concrete, dissolved carbonates in mix water may serve as sources of carbonate ions. There is a clear difference in calcium carbonate fraction of both concrete mixes made with OPC and RM, which can be identified on the XRPD map at 29.6° 2θ (Powder diffraction file 00-005-0586, ICDD). The significantly low fraction of calcium carbonate in OPC could be due to the formation of a higher fraction of thaumasite as compared to RM blended concrete.

Calcium chloride forms calcium hypochlorite by consuming the portlandite in the presence of water. It can be identified at 39.4° 2θ (Powder diffraction file 00-002-0280, ICDD) on the XRPD map. As compared to concrete made with OPC, calcium hypochlorite peak intensity is significantly higher in concrete made with RM. Calcium hypochlorite has the potential to decrease the pH of pore solution by consuming hydrated $Ca(OH)_2$ and thus causes the corrosion of rebar [33, 34]. It indicated that the high I_{corr} value of rebar in concrete with RM, as shown in Fig. 8, is due to high amounts of calcium hypochlorite. The XRPD map of concrete made with OPC and RM indicates that the peak intensity of $Ca(OH)_2$ at 36.55° 2θ (COD database: 96-100-1788) is lesser in concrete with RM as compared to those made with OPC. Therefore, from the XRPD analysis, the concrete with RM shows significantly lower pH due to the consumption of $Ca(OH)_2$ and leads to more corrosion of rebar as compared to the rebar in OPC., for w/cm ratio 0.51. Due to the aggregates present in concrete, the peaks corresponding to Quartz can be identified at 20.85° 2θ, 26.61° 2θ, 42 .42° 2θ, 50.1°, 54.8° 2θ, 59.86° 2θ, 68.2°2θ (Powder diffraction file 00-046-1045, ICDD) in concrete with OPC and RM for w/cm ratio 0.51.

Discussion

As per the corrosion potential versus time plot (Fig. 4), the corrosion has been initiated before 60 days age of concrete. However, at the age of 60 days I_{corr} values of rebar embedded in concrete made with OPC and RM for w/cm 0.51 are 2.5 µA/cm^2 and 1.5 µA/cm^2, respectively, and for w/cm ratio 0.48, these values are 0.76 µA/cm^2 and 0.3 µA/cm^2, respectively. Significantly higher I_{corr} values and lower electrical resistivity of slab specimens also confirmed concrete corrosion at 60 days of age. This can be due to the addition of calcium chloride during concrete preparation. The presence of high chloride content at initial days leads to high rebar corrosion and low electrical resistivity of concrete.

The variation of potential, I_{corr}, and concrete resistivity values over the period of 420 days can be observed due to the

changes in concrete microstructure over the period of time. While observing the trend of both potential and I_{corr} values of rebar in OPC and RM blended concrete made with w/cm 0.48 and 0.51, no unambiguous relation has been observed. After reaching the maximum negative potential value in all concrete mixes, the potential values tend toward positive, during which there is no significant change in I_{corr}, value. In order to investigate the relation between potential values and I_{corr} values, the scatter plot has been drawn between them, as shown in Fig. 9. From Fig. 9, it is confirmed that there is no correlation exists between the potentials and I_{corr}, values. This can be due to the composition of rust formed on the rebar effects the potential values. However, various aging of the rust (proportion Fe^{+2}/Fe^{+3}) induce various potential values for the same corrosion current density values [35]. The trend of the potentials toward to the positive direction may be due to the corrosion products deposited on rebar surface.

In order to correlate the behavior of I_{corr} data with electrical resistivity measured by IR compensation, the scatter plot of I_{corr} versus electrical resistivity was drawn, as shown in Fig. 10. According to Fig. 10, no general correlation has been observed between I_{corr} value and electrical resistivity of concrete contaminated with $CaCl_2$. However, it is essential to consider the range of electrical resistivity of concrete specimens in the present study, as previous literature [36, 37] reported that resistivity is not a controlling parameter for the corrosion of the rebar if the concrete resistivity is less than 10 kΩ cm. As the resistivity of all concrete specimens was lower than 10 kΩ cm, concrete resistivity is not controlling factor of the corrosion rate. Therefore, for the corrosion process, although ionic transport is required by concrete pore solution, the concrete resistivity is not the controlling factor of rebar corrosion at high conductivity of concrete. The

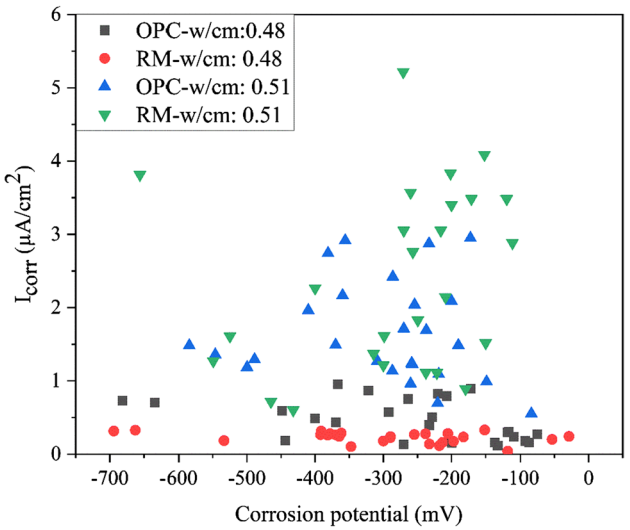

Fig. 9 Scatter plot of corrosion current density and corrosion potential

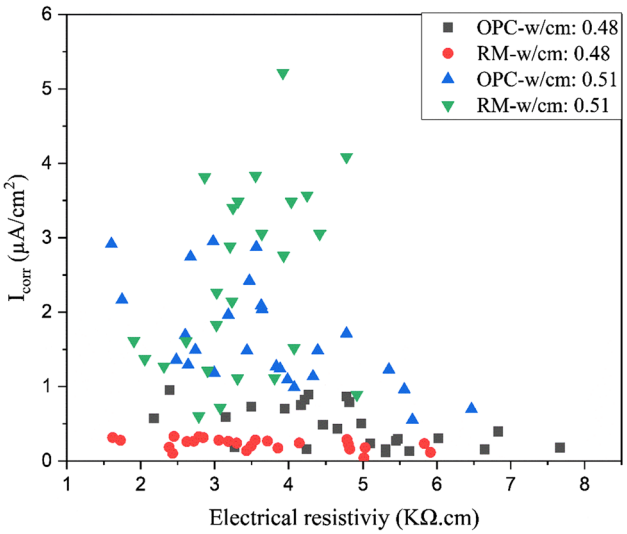

Fig. 10 Scatter plot of corrosion current density and electrical resistivity

presence of significant chlorides in the concrete can be due to the high conductivity and low resistivity of the concrete.

From the I_{corr} values, as shown in Figs. 5 and 6, the effect of RM on the rebar corrosion varies with respect to w/cm ratios of 0.48 and 0.51. According to Table 3, low and moderate corrosion levels were observed on rebar embedded in RM and OPC concrete, respectively, in the case of w/cm 0.48 over a period of 420 days, whereas in the case of w/cm 0.51 higher corrosion levels were observed in both types of concrete. The lower corrosion of the rebar in the concrete blended with RM as compared to OPC concrete for the w/cm 0.48 may be due to the filler effect of RM in concrete [12]. For w/cm 0.51, rebar in concrete made with RM performed better than those embedded in OPC concrete up to 210 days; after that, the trend was different. This can be attributed to the changes in concrete pore solution chemistry. In order to understand the high corrosion activity of rebar in concrete, X-ray powder diffraction analysis was conducted on concrete powder collected from the steel–concrete interface of slab specimens made for w/cm 0.51. From the XRPD map, the higher corrosion of rebar embedded in RM blended concrete

Table 3 Classification of the level of corrosion based on corrosion current density [36]

Corrosion current density (μA/cm^2)	Corrosion level
< 0.1	Negligible
0.1–0.5	Low
0.5–1	Moderate
> 1	High

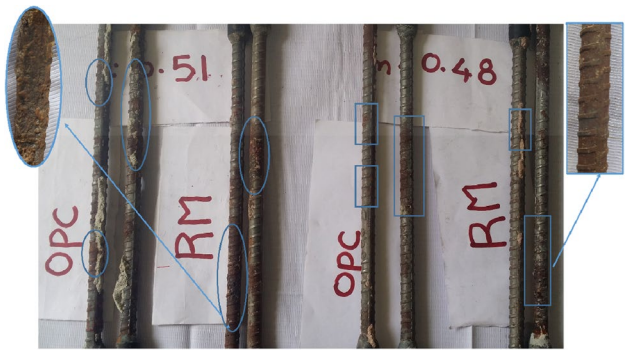

Fig. 11 Visual observation of rebars in concrete with w/cm 0.51 and 0.48

with w/cm 0.51 can be attributed to a higher fraction of calcium hypochlorite.

While observing the overall performance of RM blended concrete on rebar corrosion, in case of w/cm 0.51 RM blended concrete increased the corrosion as compared to OPC concrete for the same chloride content. On the other hand, for w/cm 0.48 RM blended concrete decreased the corrosion of rebar as compared to OPC concrete. This can be evident from the visual observation of rebar, which was taken out from the slab specimens after 420 days of age. Small pits were observed on rebar embedded in concrete for w/cm 0.51, as shown in Fig. 11, whereas the brownish rust strains were observed on rebar in concrete for w/cm 0.48. Among all the rebars, severe corrosion has been observed on rebar embedded in concrete with RM with w/cm 0.51. The current investigation is limited to determine the effect of RM on the corrosion performance of embedded rebar when $CaCl_2$ is added to concrete during concrete production. This work can be extended to more variations of w/cm ratios and % of $CaCl_2$ with different sources of RM to draw more significant outcomes in near future.

Conclusions

Based on the experimental investigation and the analysis of results carried out, the following conclusions can be drawn:

1. In the case of concrete with w/cm 0.48, concrete made with 5% red mud reduces the corrosion of rebar over the test period of 420 days as compared to concrete made with OPC alone.
2. In the case of concrete made of w/cm 0.51, concrete made with red mud initially showed better performance, but this trend was reversed in concrete at later ages.
3. Corrosion current density values show no relationship between corrosion potential and IR-compensated electrical resistivity values.
4. Pits were observed on the rebar embedded in concrete made for w/cm 0.51, while brownish rust strains were observed on rebar in concrete made for w/cm 0.48, in the case of concrete made by RM.
5. For the same chloride content, the formation of high amounts of calcium hypochlorite indicates higher I_{corr} values of the rebar embedded in the concrete blended with RM as compared to OPC concrete.

Acknowledgements The authors would like to express their gratitude to National Aluminium Company Limited, Damanjodi, Orissa, India for supplying the red mud. The authors acknowledge the support provided by Civil Engineering Department, SVNIT.

Funding There was no external funding for this research.

Compliance with ethical standards

Conflict of interest The authors declare that they have no conflict of interest.

References

1. Liu Y, Naidu R (2014) Hidden values in bauxite residue (red mud): recovery of metals. Waste Manag 34:2662–2673. https://doi.org/10.1016/j.wasman.2014.09.003
2. International Aluminium Institute International Aluminium Institute. Primary aluminium production. In: World Alum. http://www.world-aluminium.org/statistics/#data. Accessed Apr 2020
3. Samal S, Ray AK, Bandopadhyay A (2013) Proposal for resources, utilization and processes of red mud in India—a review. Int J Miner Process 118:43–55. https://doi.org/10.1016/j.minpro.2012.11.001
4. Singh S, Aswath MU, Ranganath RV (2016) Durability of red mud based geopolymer paste in acid solutions. Mater Sci Forum 866:99–105. https://doi.org/10.4028/www.scientific.net/MSF.866.99
5. Díaz B, Freire L, Nóvoa XR, Pérez MC (2015) Chloride and CO2 transport in cement paste containing red mud. Cem Concr Compos 62:178–186. https://doi.org/10.1016/j.cemconcomp.2015.02.011
6. Cabeza M, Collazo A, Nóvoa XR, Pérez MC (2003) Red mud as a corrosion inhibitor for reinforced concrete. J Corros Sci Eng 6:1–4
7. Collazo A, Cristóbal MJ, Nóvoa XR et al (2006) Electrochemical impedance spectroscopy as a tool for studying steel corrosion inhibition in simulated concrete environments—red mud used as rebar corrosion inhibitor. J ASTM Int 3:1–10. https://doi.org/10.1520/JAI11785
8. Yang X, Zhao J, Li H et al (2017) Recycling red mud from the production of aluminium as a red cement-based mortar. Waste Manag Res 35:1–8. https://doi.org/10.1177/0734242X16684386
9. Venkatesh C, Ruben N, Chand MSR (2020) Red mud as an additive in concrete: comprehensive characterization. J Korean Ceram Soc. https://doi.org/10.1007/s43207-020-00030-3
10. Venkatesh C, Nerella R, Chand MSR (2020) Experimental investigation of strength, durability, and microstructure of red-mud concrete. J Korean Ceram Soc. https://doi.org/10.1007/s43207-019-00014-y
11. Nikbin IM, Aliaghazadeh M, Charkhtab S et al (2016) Environmental impacts and mechanical properties of lightweight concrete

containing bauxite residue (red mud). J Clean Prod 172:2683–2694. https://doi.org/10.1016/j.jclepro.2017.11.143
12. Manfroi EP, Cheriaf M, Rocha JC et al (2014) Microstructure, mineralogy and environmental evaluation of cementitious composites produced with red mud waste. Constr Build Mater 67:29–36. https://doi.org/10.1016/j.conbuildmat.2013.10.031
13. Ribeiro DV, Labrincha JA, Morelli MR (2012) Effect of the addition of red mud on the corrosion parameters of reinforced concrete. Cem Concr Res 42:124–133. https://doi.org/10.1016/j.cemconres.2011.09.002
14. Collepardi M, Coppola L, Pistolesi C (1994) Durability of concrete structures exposed to CaCl2 based deicing salts. Spec Publ 145:107–120
15. Chatterji S (1978) Mechanism of the CaCl2 attack on portland cement concrete. Cem Concr Res 8:461–467. https://doi.org/10.1016/0008-8846(78)90026-1
16. Li C, Jiang L, Li S (2020) Effect of limestone powder addition on threshold chloride concentration for steel corrosion in reinforced concrete. Cem Concr Res 131:106018. https://doi.org/10.1016/j.cemconres.2020.106018
17. Delagrave A, Marchand J, Ollivier JP et al (1997) Chloride binding capacity of various hydrated cement paste systems. Adv Cem Based Mater 6:28–35. https://doi.org/10.1016/S1065-7355(97)90003-1
18. Balonis M, Lothenbach B, Le G et al (2010) Cement and concrete research impact of chloride on the mineralogy of hydrated Portland cement systems. Cem Concr Res 40:1009–1022. https://doi.org/10.1016/j.cemconres.2010.03.002
19. Roberts MH (1962) Effect of calcium chloride on the durability of pre-tensioned wire in prestressed concrete. Mag Concr Res 14:143–154
20. ASTM G109-99a (2005) Standard test method for determining the effects of chemical admixtures on the corrosion of embedded steel reinforcement in concrete exposed to chloride environments
21. ASTM C876-09 (2009) Standard test method for corrosion potentials of uncoated reinforcing steel in concrete. ASTM Int, West Conshohocken
22. Raghu Babu U, Kondraivendhan B (2019) Impact of sulphate on chloride-induced corrosion of steel in concrete. Indian Concr J 93:8–17
23. Raghu Babu U, Kondraivendhan B (2020) Corrosion performance of steel reinforcement in concrete admixed with magnesium chloride and sulphate. Anti Corr Methods Mater 67:106–118. https://doi.org/10.1108/ACMM-08-2019-2163
24. Liu G, Zhang Y, Wu M et al (2018) Electrochemical analysis of carbon steel corrosion induced by chloride and sulfate ions in simulated concrete pore solution. Int J Electrochem Sci 13:6248–6258. https://doi.org/10.20964/2018.07.46
25. Vedalakshmi R, Manoharan S, Song HW, Palaniswamy N (2009) Application of harmonic analysis in measuring the corrosion rate of rebar in concrete. Corros Sci 51:2777–2789. https://doi.org/10.1016/j.corsci.2009.07.014
26. Ahmad S, Bhattacharjee B (1995) A simple arrangement and procedure for in situ measurement of corrosion rate of rebar embedded in concrete. Corros Sci 37:781–791. https://doi.org/10.1016/0010-938X(95)80008-5
27. Samson G, Deby F, Garciaz J-L, Perrin J-L (2018) A new methodology for concrete resistivity assessment using the instantaneous polarization response of its metal reinforcement framework. Constr Build Mater 187:531–544. https://doi.org/10.1016/j.conbuildmat.2018.07.158
28. Pradhan B, Bhattacharjee B (2011) Rebar corrosion in chloride environment. Constr Build Mater 25:2565–2575. https://doi.org/10.1016/j.conbuildmat.2010.11.099
29. Vedalakshmi R, Rajagopal K, Palaniswamy N (2009) Durability performance of rebar embedded in chloride admixed blended cement concretes. Corros Eng, Sci Technol 46:256–270. https://doi.org/10.1179/174327809x409204
30. Sadowski L (2013) Non-destructive investigation of corrosion current density in steel reinforced concrete by artificial neural networks. Arch Civ Mech Eng 13:104–111. https://doi.org/10.1016/j.acme.2012.10.007
31. Sadowski L (2010) New non-destructive method for linear polarisation resistance corrosion rate measurement. Arch Civ Mech Eng 10:109–116. https://doi.org/10.1016/s1644-9665(12)60053-3
32. Langford P, Broomfield J (1987) Monitoring the corrosion of reinforcing steel. Palladian Publications Ltd, Farnham
33. Zhu Q, Jiang L, Chen Y et al (2012) Effect of chloride salt type on chloride binding behavior of concrete. Constr Build Mater 37:512–517. https://doi.org/10.1016/j.conbuildmat.2012.07.079
34. Das JK, Pradhan B (2019) Effect of cation type of chloride salts on corrosion behaviour of steel in concrete powder electrolyte solution in the presence of corrosion inhibitors. Constr Build Mater 208:175–191
35. Andrade C, Alonso C (2004) Test methods for on-site corrosion rate measurement of steel reinforcement in concrete by means of the polarization resistance method. Mater Struct 37:623–643. https://doi.org/10.1007/BF02483292
36. Andrade C, Alonso C (2001) On-site measurements of corrosion rate of reinforcements. Constr Build Mater 15:141–145. https://doi.org/10.1016/S0950-0618(00)00063-5
37. Andrade C, Alonso C (1996) Corrosion rate monitoring in the laboratory and on-site. Constr Build Mater 10:315–328